Polymer 51 (2010) 3277–3284

Contents lists available at ScienceDirect

Polymer

journal homepage: www.elsevier.com/locate/polymer

The toughening mechanism of polypropylene/calcium carbonate nanocomposites

Yong Lin [a], Haibin Chen [b], Chi-Ming Chan [a,c,*], Jingshen Wu [b]

[a] Department of Chemical and Biomolecular Engineering, The Hong Kong University of Science and Technology, Clear Water Bay, Hong Kong
[b] Department of Mechanical Engineering, The Hong Kong University of Science and Technology, Clear Water Bay, Hong Kong
[c] Division of Environment, The Hong Kong University of Science and Technology, Clear Water Bay, Hong Kong

ARTICLE INFO

Article history:
Received 7 October 2009
Received in revised form
21 April 2010
Accepted 23 April 2010
Available online 29 April 2010

Keywords:
Polypropylene
Calcium carbonate
Nanocomposites

ABSTRACT

The toughening mechanism of polypropylene (PP) filled with calcium carbonate ($CaCO_3$) nanoparticles is described. In a previous study (Macromolecule 2008;41:9204), we observed that intensive ligament-stretching following debonding of nanoparticles was responsible for the significant improvement in the impact toughness of the annealed PP/$CaCO_3$ nanocomposites. Furthermore, we hypothesized that strong ligaments, which have high fracture stresses, are needed to stabilize the crack-initiation process and to increase the energy dissipation in the crack-initiation stage. In this study, we used a high-molecular-weight PP to test this hypothesis because strong ligaments could be created from this high-molecular-weight PP. The notched Izod impact strength of the nanocomposites containing the high-molecular-weight PP and 20 wt% $CaCO_3$ nanoparticles with a monolayer coating of stearic acid was measured to be about 370 J/m, whereas the impact strength of the unfilled PP was 50 J/m. The size of the plastic deformation zone was found to be dependent on the molecular weight of the PP matrix because the strong ligaments of the high-molecular-weight PP enabled the expansion of the plastic deformation zone, leading to a considerable increase in the impact strength. The synergic effect of the high-molecular-weight PP and the monolayer-coated nanoparticles produced nanocomposites with high impact strength, which is much greater than the inherent impact strength of the unfilled polymer. In addition, the effect of the high-molecular-weight PP on the dispersion of the nanoparticles was investigated.

1. Introduction

Mechanical performance of polymers can be significantly improved by the incorporation of inorganic nanoparticles [1–3]. For instance, the stiffness and toughness of polypropylene (PP) can be increased by the addition of calcium carbonate ($CaCO_3$) nanoparticles [4]. Nanocomposites of PP/$CaCO_3$ have attracted much research interest, leading to the publication of many papers about their toughening mechanisms [4–14]. Kim et al. [5,6] studied the in-situ micro-deformation process of thin films (up to several micrometers thick) of various PP composites by a scanning electron microscope (SEM) and a high-voltage electron microscope. The micro-deformation processes varied with the phase morphology of the modifier particles and the adhesion between the modifier particles and the polymer matrix [5,6]. Debonding followed by shear yielding of PP was identified as the micro-deformation process in the microsized-$Al(OH)_3$ particle filled PP composite [5,7]. It should be emphasized that the micro-deformation processes they observed happened in thin-film samples deformed in a uniaxial tension at low speeds. The micro-deformation process of bulk materials may vary under high strain rates. Under such circumstances, the strain constraint is high and shear yielding usually cannot take place, resulting in brittle fracture [15]. For example, the toughening effect of micro-particles in bulk PP was minimal because massive plastic deformation was absent during impact loading [16,17]. It was however later shown that 700-nm $CaCO_3$ particles could improve the Izod impact strength of PP [8,9]. Zuiderduin and Gaymans [8] suggested that the above mentioned micro-deformation process, debonding and shear yielding, were responsible for the improved impact toughness of the bulk PP. They concluded the toughening mechanism of the PP nanocomposite by putting forward the concept of the 'three-stage mechanism' proposed by Kim and Michler [7]. The inorganic particles serve as stress concentrators to build up a stress field around themselves. Given the weak adhesion between the particles and the polymer matrix, debonding at the particle–matrix interface would take place, leading to the release of the strain constraints at the crack tip and consequent massive plastic deformation, which consumed a large amount of energy [8]. This toughening mechanism, which was valid for PP filled with sub-micrometer (700 nm) $CaCO_3$

* Corresponding author. Division of Environment, The Hong Kong University of Science and Technology, Clear Water Bay, Hong Kong. Tel./fax: +852 2358 7125.
E-mail address: kecmchan@ust.hk (C.-M. Chan).

0032-3861/$ – see front matter © 2010 Elsevier Ltd. All rights reserved.
doi:10.1016/j.polymer.2010.04.047

particles [8], was once controversial in the case of $CaCO_3$ nanoparticles (particle size below 100 nm). The toughening effects of the nanoparticles were usually confounded with adverse agglomeration. Good dispersion of nanoparticles is essential for any investigation on the toughening mechanisms of nanocomposites. In our previous study [18], we achieved good dispersion of $CaCO_3$ nanoparticles in a PP matrix by treating the nanoparticles with a monolayer coating of stearic acid. Furthermore, we reported that the impact strength of PP/$CaCO_3$ nanocomposites increased substantially upon annealing. The detailed study on the annealed nanocomposite samples showed that the intensive stretching of PP ligaments, which occurred after the debonding of nanoparticles at the crack-initiation stage, was responsible for the high impact toughness. This is the first-time observation to confirm the occurrence of the debonding of the nanoparticles and the consequent massive plastic deformation in the PP/$CaCO_3$ nanocomposites. Although the micro-deformation process and the toughening mechanism are basically the same for nanocomposites and microcomposites, nanoparticles are expected to have better toughening effects than micro-particles because nano-voids are more stable than micro-voids. Moreover, we observed that little energy was consumed during the crack propagation and the collective collapse of the ligaments at the crack tip determined the onset of the catastrophic crack propagation. We therefore hypothesized that the ligament strength, which refers to the strength level at which ligaments fracture, is crucial because it determines the dimensions of the plastic deformation zone developed at the crack-initiation stage and consequently the impact toughness.

In this study, we investigated the effects of ligament strength on the impact toughness of PP/$CaCO_3$ nanocomposites with the aim to gain insights into the toughening mechanism. The ligament strength was varied by using PPs with different molecular weights. Ishikawa et al. showed that the strength of oriented PP fibrils increased with molecular weight [19]. They attributed the high fracture stress of the high-molecular-weight PP to the high concentration of tie molecules. Ligaments in nanocomposites are similar to the oriented fibrils of neat PP in terms of their microstructure and morphology. The strength of the ligaments is reasonably assumed to be a function of the concentration of the tie molecules, which depends on the molecular weight of the polymer matrix.

There have been many studies on the effects of molecular weight on the mechanical properties of various polymer composites [8,20–27]. The functions of the high-molecular-weight matrix differ in various systems. For example, in organoclay-filled nylon 6, the major role of the high-molecular-weight matrix is to provide high shear forces to disperse organoclay during melt-blending [23]. Paul et al. [24–26] performed a systematical study on the role of the molecular weight of the matrix in the rubber-toughened nylon 6 blends. They observed that the high-molecular-weight matrix reduced the sizes of the rubber particles, leading to the enhancement of impact toughness [24]. Furthermore, the impact toughness of nylon 6 blends increased with molecular weight when the rubber particle sizes were kept constant, implying that in addition to reduce the particle size, the inherent high impact toughness of the high-molecular-weight matrix was also beneficial [25,26]. Actually, the increase of the impact toughness of composites with matrix molecular weight was commonly observed in rubber-filled PP [27] as well as $CaCO_3$-filled PP composites [8]. Zuiderduin and Gaymans [8] attributed the high impact toughness of high-molecular-weight PP composites to the high inherent ductility of the neat PP, or the ability to be toughened (i.e., toughenability). Although these results are intuitively expected, the exact mechanism has not been fully understood. The conclusions drawn in this paper not only confirm the importance of strong ligaments to the impact toughness of the nanocomposites, but also explain the concept of 'better toughenability' in terms of the micro-structure. In addition, the effects of molecular weight on the dispersion of nanoparticles were examined.

2. Experimental

2.1. Materials

Two kinds of homopolymer isotactic PPs (i-PP) were used in this study. One was HJ730L (H-PP, number-average molecular weight ($\overline{M}_n$) = 55,000 g/mol; weight-average molecular weight ($\overline{M}_w$) = 346,000 g/mol) from Samsung Company. The other PP (E-PP) was a high-molecular-weight polymer ($\overline{M}_n$ = 88,000 g/mol; $\overline{M}_w$ = 472,000 g/mol) supplied by Japan Polypropylene. The melt flow indexes of H-PP and E-PP were measured to be 5.0 g/10 min (ASTM D1238) and 0.5 g/10 min (JIS 7210-1999 standard), respectively. Calcium carbonate nanoparticles with the trade name of SPT were provided by Solvay Chemicals. SPT was surface-modified with stearic acid as received. The diameter of the nanoparticles was around 70 nm and their micro-morphology was shown in a previous paper [18]. Stearic acid with a purity of 95% was purchased from Sigma. An anti-oxidant, Irganox 1010 (0.5 wt%), was added to the PP during compounding.

2.2. Preparation of PP/$CaCO_3$ nanocomposites

The as-received nanoparticles were further treated with stearic acid to produce a monolayer coating. The surface treatment was conducted in a mixture of ethanol and water at 80 °C for 2 h. The detailed procedures were described in a previous paper [18]. The as-received and monolayer-coated nanoparticles were coated with 2.3 and 5.3 wt% stearic acid, respectively, as determined by thermogravimetric analyses [18]. Nanocomposites were prepared by blend-mixing 20 wt% nanoparticles with either H-PP or E-PP at 180 °C, using a Haake mixer. A special nanocomposite, named MA-5-20, was prepared by compounding E-PP with 40 wt% monolayer-coated nanoparticles for 15 min to produce a concentrated master batch and then the nanoparticle concentration was adjusted to 20 wt% by blending with H-PP for another 15 min. The detailed compounding procedures can be found elsewhere [4]. Table 1 shows the compositions of the nanocomposites used in this study.

2.3. Material characterization

The crystallization characteristics of the nanocomposites were studied by a Perkin Elmer (Diamond 7) differential scanning calorimeter (DSC). The crystallization temperature (T_c) and melting temperature (T_m) of the samples taken from the impact bars were detected at cooling and heating scans, respectively, at a rate of 10 °C/min. The crystallinity of the samples was measured with the heating scans, based on the assumption that the heat of fusion of the PP crystals was 209 J/g [28]. The surface of impact-fractured samples was observed on a JOEL JSM-6700F SEM. The size of the plastic deformation zone was measured at the cross-section of the

Table 1
Composition (wt%) of the nanocomposites.

Sample	H-PP	E-PP	$CaCO_3$
H-2-20	80	0	20 (2.3 wt% surfactant)
H-5-20	80	0	20 (5.3 wt% surfactant)
E-2-20	0	80	20 (2.3 wt% surfactant)
E-5-20	0	80	20 (5.3 wt% surfactant)
MA-5-20	50	30	20 (5.3 wt% surfactant)

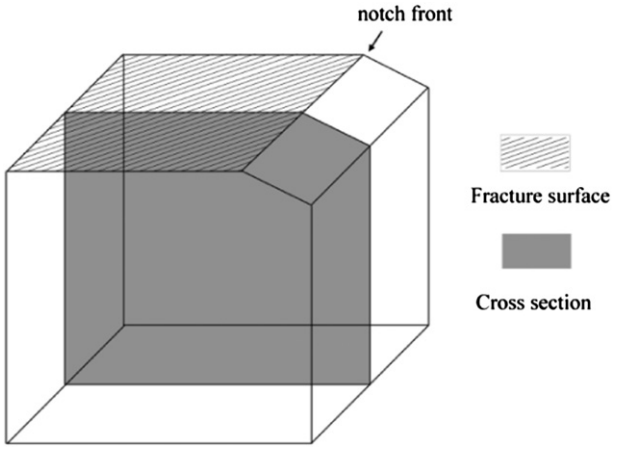

Fig. 1. Schematic of the fracture surface and the core cross-section of a broken Izod impact bar for SEM observations [18].

impact-fractured sample, as schematically shown in Fig. 1. The broken Izod impact bar was immersed in liquid nitrogen for more than 20 min. Then it was cleaved immediately by a wedge to produce the cross-section (less than 3 s) after it had been taken out of liquid nitrogen.

2.4. Mechanical tests

The injection molding conditions of the tensile and impact bars were described previously [4]. The tensile and notched Izod impact tests were conducted in accordance with ASTM-D658 and ASTM-D256, respectively. The tensile bars were stored at 23 ± 3 °C at a relative humidity of 50% for 24 h before testing. The tensile test was performed on an Instron testing machine and the crosshead speed was 5 mm/min. The striker velocity of a impact test was around 3.5 m/s. V-shaped notches with a radius of around 0.25 mm in the impact bars were produced by a CSI automatic notcher (CS-93M). The cutter speed and the table feed rate were about 92 and 100 mm/min, respectively. The Izod impact tests were conducted one day after the samples were notched. At least five specimens were tested for one average data point in tensile and impact tests. Load-displacement curves of the nanocomposites at high strain rates were measured. The experiment was performed using a Dynatup 8250 instrumented drop-weight impact tester. The impact velocity was set to be 2.0 m/s and the drop weight (the crosshead and the tup) was 0.6 Kg. V-shaped notched specimens (ASTM-D256) were used in this Charpy-type impact test. The two ends of V-notched specimens were supported by fixtures and the middle part was suspended with the notch downward. The tup was aligned with the specimen so that the tup would hit exactly at the center of the specimens.

3. Results and discussion

3.1. Crystallization behaviors of the PPs and their nanocomposites

The crystallization behaviors of the two PPs and their nanocomposites were studied by DSC. Fig. 2a and b show the crystallization and melting curves, respectively. As shown in Fig. 2a, E-PP has the lowest T_c because its high-molecular-weight hinders the crystallization process [29,30]. The $CaCO_3$ nanoparticles exhibit good nucleating effects, as evidenced by the fact that the T_c of the nanocomposites was about 6 °C higher than the T_c of their corresponding unfilled PPs. The T_ms of the nanocomposites were higher than those of the unfilled samples possibly due to the onsets of crystallization of the nanocomposites at higher temperatures, leading to a larger average lamellar thickness. For example, the T_m of H-5-20 was 2 °C higher than that of E-5-20, indicating that the average lamellar thickness of H-5-20 was slightly larger. The small peaks at 143 and 151 °C in the melting curve of H-5-20 are the endothermic peaks of the β phase. Actually, both E-PP and E-5-20 also have a small amount of β phase, but the melting peaks of the β phase are quite weak, as indicated by arrows in Fig. 2b. The crystallinity of the samples is listed in Table 2. With the addition of $CaCO_3$ nanoparticles, the degree of crystallinity of PPs varied only slightly.

3.2. Tensile properties of the PPs and their nanocomposites

The stress–strain relationships of H-PP and E-PP and their nanocomposites were studied. Selected tensile properties are listed in Table 3 and the representative stress–strain curves of the samples are shown in Fig. 3. For clarity, each curve was shifted to the right by 0.5 units from its preceding one. The Young's modulus and the tensile yield stress of E-PP are higher than those of H-PP in spite of the fact that the crystallinity of H-PP is higher than that of E-PP. The Young's modulus of a polymer depends not only on the degree of crystallinity but also on the crystalline orientation [31,32]. The degree of the melt orientation during injection molding enhances as the molecular weight increases, leading to an increased extent of the *c*-axis orientation of the polymer chains in the tensile-test direction. The skin layer of an injection-molded sample had a shish-kebab structure and the thickness of this skin layer increased with molecular weight of the polymer [33,34]. These orientation effects explain the higher Young's modulus of E-PP. The yield stress is controlled by the thickness of the lamellae

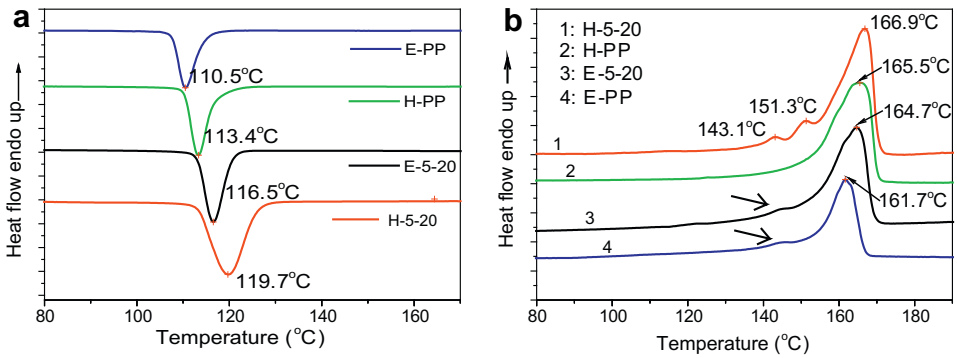

Fig. 2. Crystallization (a) and melting (b) curves of the two PPs and their nanocomposites.

Table 2
Crystallinity of the PPs and their nanocomposites determined with DSC.

Sample	E-PP	H-PP	E-5-20	H-5-20
Crystallinity	30.3	34.6 [18]	33.5	33.3 [18]

[35] as well as the connectivity of the inter-lamellae and inter-spherulites [36]. A high-molecular-weight PP generally has a high concentration of tie molecules, which go through adjacent lamellae and spherulitic boundaries. A higher stress level is needed for crystal fragmentation in a PP with a well-connected network [37]. Therefore, the higher tensile yield stress of E-PP is reasonable regardless of its slightly lower crystallinity. The Young's moduli of all the nanocomposites were improved compared with their unfilled counterparts due to the addition of rigid $CaCO_3$ nanoparticles. However, the tensile yield stresses of E-5-20 and H-5-20 decreased by 10% compared with the corresponding neat PPs, suggesting that debonding between the nanoparticles and the polymer matrix occurred before yielding. As a result, the release of the strain constraint lowered the tensile yield stress. In addition, the lower yield strain of the nanocomposites is also indicative of the occurrence of debonding prior to yielding.

H-PP has a higher tensile strength than does E-PP, as shown in Fig. 3. H-PP has the most noticeable strain-hardening effect, accompanied by the highest tensile strength and the longest elongation-at-break. One of the determining factors of tensile strength is the degree of chain alignment, or in the case of tensile tests, the extent of elongation, which depends on the molecular weight. According to Peterlin's molecular model of fracture of polyethylene and PP [38], plastic deformation involves a transformation from the spherulitic structure to the micro-fibril structure, which contains unfolded crystal blocks connected with tie molecules. As the molecular weight increases, the number of tie molecules, which bridge the microfibrils, increases, restricting the flow of the microfibrils and hence reducing the draw ratio. A better inter-connected chain network of E-PP prevents a large elongation of the sample and hence reduces the orientation of the polymer chains, leading to a smaller elongation-at-break and a lower tensile strength. It is worth pointing out that that stress level of E-PP during necking is higher than that of H-PP, implying that E-PP has a stronger network of polymer chains than H-PP has. Despite the difference in the elongation-at-break between E-PP and H-PP, their nanocomposites, E-5-20 and H-5-20, actually have similar elongation-at-break values. After debonding, a micro-fibril structure is formed, which is analogous to the micro-morphology of PP during necking. Microfibrils in nanocomposites are called ligaments. Fig. 3 clearly shows that at any strain, the stress level of E-5-20 is higher than that of H-5-20. Moreover, the tensile strength of E-5-20 is noticeably higher than that of H-5-20. Since E-5-20 and H-5-20 have the same nanoparticle concentrations, the number of ligaments per unit volume in these samples can be assumed to be the same. A higher tensile strength of E-5-20 means that a single ligament of E-5-20 can withstand a higher fracture stress than can a single ligament of H-5-20. The higher stress level during necking

Table 3
Tensile properties of E-PP and H-PP and their nanocomposites.

Sample	Young's Modulus (GPa)	Yield stress (MPa)	Yield strain (%)	Tensile strength (MPa)	Elongation-at-break (mm/mm)
H-PP	1.9 ± 0.1	36.3 ± 0.1	8.1 ± 0.1	50.6 ± 6.3	8.5
E-PP	2.5 ± 0.2	39.7 ± 1.1	10.8 ± 1.1	45.7 ± 1.7	5.0
H-5-20	2.7 ± 0.1	31.6 ± 0.4	5.2 ± 0.3	31.1 ± 3.0	6.0
E–5-20	3.0 ± 0.3	36.3 ± 0.6	6.1 ± 0.3	41.6 ± 0.9	5.5

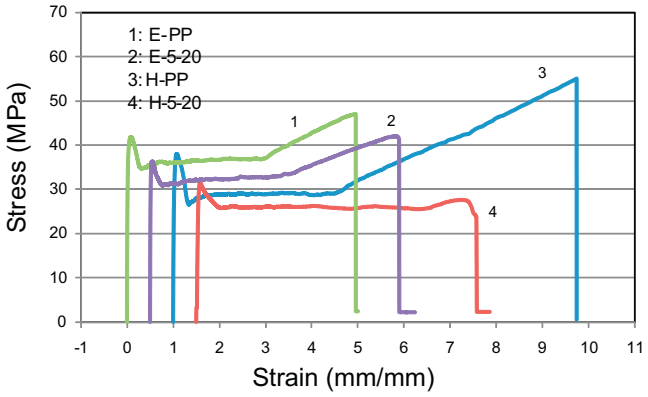

Fig. 3. Representative stress-strain curves of the two PPs and their nanocomposites.

and the higher tensile strength indicate that the ligaments of E-5-20 are stronger than are those of H-5-20.

3.3. Effect of matrix molecular weight on the dispersion state of nanoparticles

The high impact toughness of a nanocomposite with a high-molecular-weight matrix is usually attributed to the good dispersion of the nanoparticles facilitated by high shear forces during blending. To determine if the high-molecular-weight matrix is effective in the dispersion of the nanoparticles, the dispersion state of the nanoparticles in the H-PP and E-PP nanocomposites was examined. Fig. 4 shows SEM micrographs of the fracture surfaces at the notch roots of H-2-20, E-2-20, and E-5-20. The arrows indicate the crack-propagation direction. In addition to the plastic deformation, the dispersion state of the nanoparticles is also visible at the fracture surface. The nanoparticles in H-2-20 and E-2-20 were coated with 2.3 wt% stearic acid, which is less than the coating amount needed to provide monolayer coverage on the nanoparticle surface. Many large agglomerates can be found in the micrographs of H-2-20 and E-2-20, as shown in Fig. 4b and d, respectively. Fig. 4e and f exhibit good dispersion of the nanoparticles in E-PP and uniform distribution of the nanoparticles in H-PP was shown in a previous paper [18]. These results suggest that although higher shear forces, which can be generated during the compounding of a higher-molecular-weight PP, can improve the dispersion to a certain extent. However, this does not guarantee good dispersion of nanoparticles. In contrast, when the nanoparticles were coated with a monolayer of stearic acid, good dispersion was achieved in spite of the difference in the molecular weight of the matrix because the surface tension of and the interactions among the nanoparticles are minimized with the monolayer coating [39].

3.4. Effect of ligament strength on impact toughness of PP/$CaCO_3$ nanocomposites

A high-molecular-weight matrix does not necessarily ensure good dispersion of nanoparticles. In addition, good dispersion alone does not necessarily ensure high impact strength. Fig. 5 show the notched Izod impact strength of neat PPs and their nanocomposites. Both H-5-20 and E-5-20 contained well-dispersed nanoparticles. However, the impact strength of H-PP only slightly increased by 20% with the addition of the nanoparticles whereas the impact strength of E-PP increased by 740%. It is important to note that the intrinsic toughness of the E-PP is higher than that of H-PP only by 25%. The fact that the impact strength of E-5-20 is six times higher than that of H-5-20 cannot be due to the matrix only.

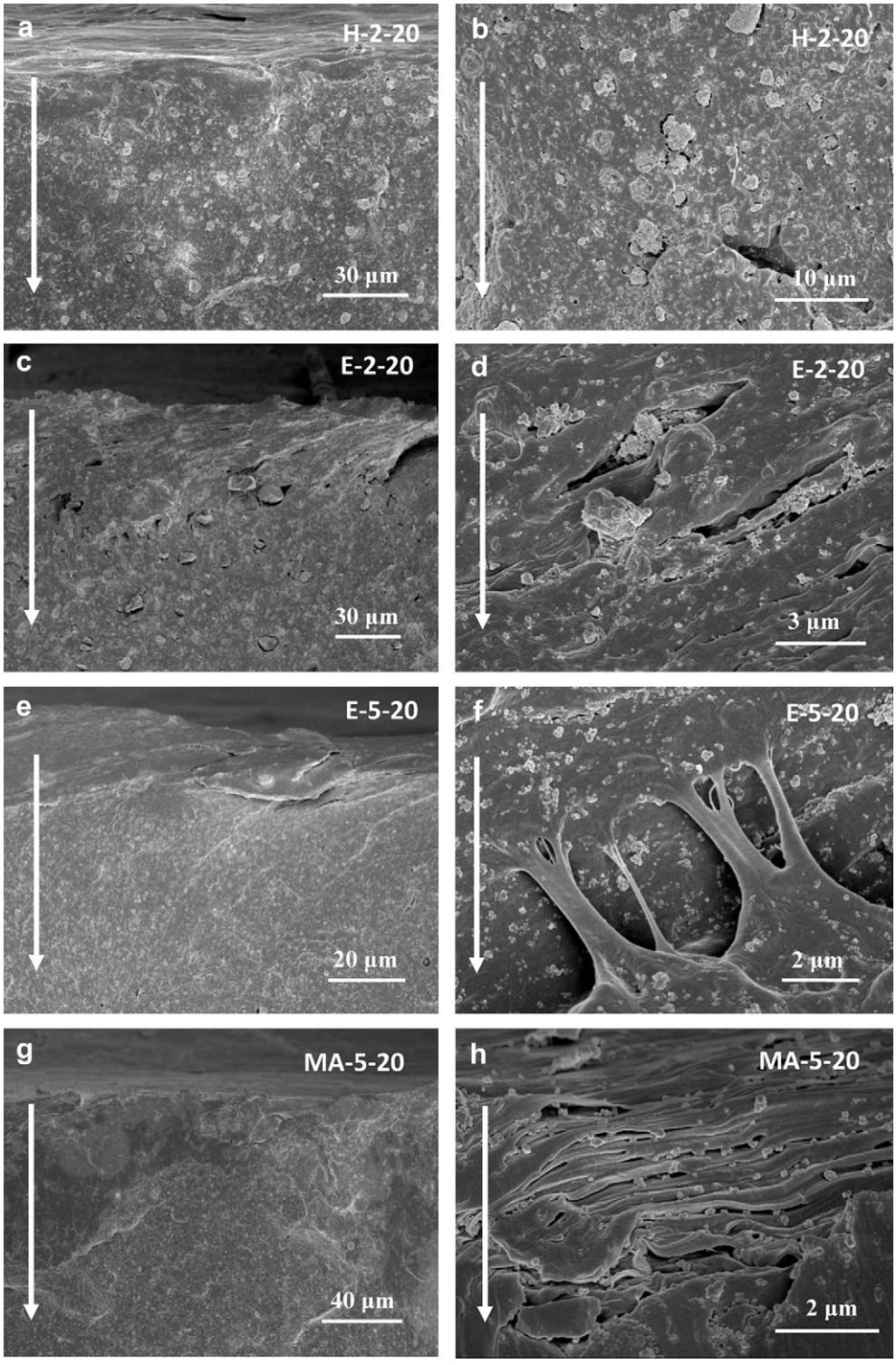

Fig. 4. SEM micrographs on the notch roots of the impact-fractured surfaces of nanocomposites. (a) and (b) H-2-20; (c) and (d) E-2-20; (e) and (f) E-5-20; and (g) and (h) MA-5-20. (b), (d), (f) and (h) are the enlarged views in the vicinity of notch roots.

There is a synergic effect of the high-molecular-weight matrix and the monolayer-coated nanoparticles on the impact strength of the nanocomposites. To further confirm this synergic effect, we used a 'two-step-blending' method, as described in the experimental section, to produce a special nanocomposite (named MA-5-20) with the matrix possessing a molecular weight between those of E-PP and H-PP. The state of the dispersion of the nanoparticles in MA-5-20, which can be viewed in Fig. 4g and h, is as good as that in E-5-20. When good dispersion was achieved in both MA-5-20 and E-5-20, the dispersion effect due to the difference in the molecular weight could be neglected while the effects of the molecular weight on the impact strength could be studied. The notched Izod impact strength of MA-5-20 containing 30 wt% E-PP and 50 wt% H-PP was 92 J/m, which was about one-fourth that of E-5-20.

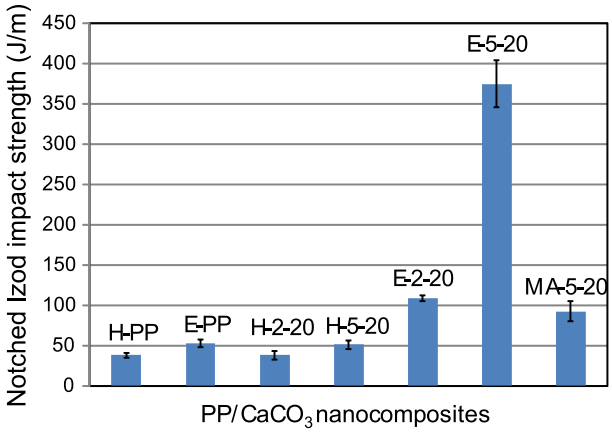

Fig. 5. Notched Izod impact strength of the PPs and their nanocomposites.

The load-displacement curves of the nanocomposites at a high strain rate were measured to reveal the toughening mechanism and the curves are shown in Fig. 6. The curves of H-5-20, MA-5-20 and E-5-20 are similar and exhibit the features of semi-brittle fracture behavior. The load rises up to a maximum value and then declines quickly. This indicates that most fracture energy was consumed in the crack-initiation stage whereas the crack propagation only contributed a small proportion of energy consumption. It is noted that the maximum load increases with the matrix molecular weight of the nanocomposites. E-5-20 has highest load and the largest displacement.

The notch roots of the Izod impact-fractured specimens were examined with a SEM to identify the plastic deformation at the crack-initiation stage. Only tiny signs of plastic deformation were observed at the fracture surfaces of MA-5-20 and E-5-20, as shown in Fig. 4f and h. However, any traces of plastic deformation can be better detected in the cross-section underneath the fracture surface at the notch roots. Fig. 7 shows the cross-sections underneath the fracture surfaces of E-5-20 and MA-5-20. A schematic picture showing the location of the sampling with respect to the impact bar is presented to the left of Fig. 7a. Letters b and c in Fig. 7a show the locations from where Fig. 7b and c were taken, respectively. Letters e and f in Fig. 7d show the locations from where Fig. 7e and f were taken, respectively. The arrows indicate the crack-propagation direction. The morphology of Fig. 7b appears to be the result of the melt flow of the polymer, possibly due to the adiabatic impact process. As revealed by the highly fibrillated ligaments (c.f., Fig. 7c), extensive plastic deformation is

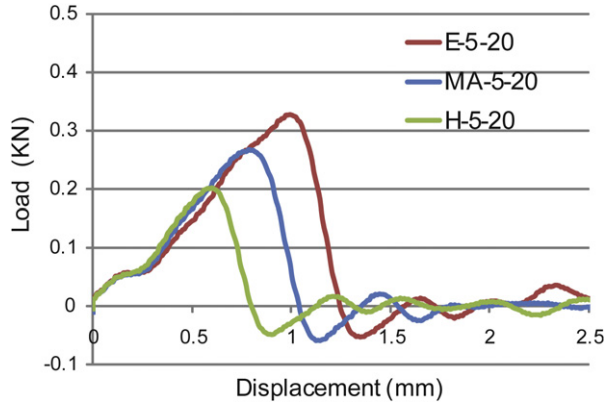

Fig. 6. Load-displacement curves of the nanocomposites at the impact velocity of 2 m/s.

obvious in E-5-20. The depth of the plastic deformation zone of this fractured sample is at least 40 μm beneath the fracture surface and the length of the plastic deformation zone is over 180 μm, as indicated in Fig. 7a. In contrast, the extent of the plastic deformation in MA-5-20 is moderate. The plastic deformation is restricted to a small region very close to the notch tip. The nanoparticles in MA-5-20 were aligned in the notch root, indicating that the ligaments were highly stretched during impact loading (c.f., Fig. 7e). Tens of micrometers away from the notch root, debonding with small dilation was found (c.f., Fig. 7f). The cross-section of H-5-20 essentially exhibits the feature of brittle fracture, which was reported in our previous paper [18]. The SEM results of H-5-20, MA-5-20 and E-5-20 are consistent with the impact strength data. E-5-20, which has the highest molecular weight matrix, can sustain the highest fracture stress and have the largest plastic deformation zone.

It is well-known that the toughness of PP increases with its molecular weight [29,40–42]. However, it should be emphasized that the increase in the impact strength of the nanocomposite with a high-molecular-weight matrix is much larger than the increase in the intrinsic impact strength of the corresponding neat PPs. For example, the impact strength of E-PP is 1.2 times higher than that of H-PP whereas the impact strength of E-5-20 is about 7.5 times higher than that of H-5-20. Obviously, the exceedingly high impact strength of E-5-20 is not mainly due to the additional energy required to rupture a single ligament of E-PP whose fracture stress is higher than that of H-PP. The load-displacement curves and the SEM observations at the notch roots of broken Izod impact bars reveal that a large part of the fracture energy originates from the enlarged volume of the matrix that involved in the plastic deformation during the crack-initiation stage.

A plastic deformation zone is built up at the crack tip of a neat polymer when subjected to an external loading. Given the validation of the linear elastic fracture mechanics, the ultimate dimensions of the plastic zone developed at fracture increase with the critical stress-intensity factor (K_{IC}) of a polymer, as analyzed in Irwin's [43] or Dugdale's [44] mode. Further, it was proven that the K_{IC} of PP increased with its molecular weight [42,45,46]. Hence, the plastic zone in the nanocomposites is theoretically predicted to increase with the molecular weight of PP, although the estimation of the size of the plastic deformation zone in PP/$CaCO_3$ nanocomposites by Irwin's or Dugdale's model may not be entirely appropriate because of the changes in the stress distribution due to the presence of nanoparticles. Nevertheless, experimental results are consistent with the theoretical deduction. The SEM observations on the notch roots of the impact-fractured samples indicate that the size of the plastic deformation zone increases with the molecular weight of the matrix. The correlation between the extent of the plastic deformation and the matrix molecular weight is established based on the fact the ligament strength increases as the molecular weight increases. As revealed by the load-displacement curves shown, as in Fig. 6, E-5-20 withstands a higher fracture stress than H-5-20 and MA-5-20, indicating the ligaments of E-5-20 are stronger due to its higher molecular weight matrix. Stronger ligaments enhance the resistance to the formation of a macro-crack and allow for the expansion of the plastic deformation zone. Consequently, the higher impact strength of E-5-20 mainly originates from a larger plastic deformation zone implemented by stronger ligaments. In addition, a comparison between the impact strengths of E-2-20 and E-5-20 demonstrates the crucial role of good dispersion of the nanoparticles. The large increase in the impact strength of PP/$CaCO_3$ nanocomposites as the molecular weight increases indicates that there is a synergic effect of a high-molecular-weight matrix and the monolayer-coated nanoparticles on the impact strength.

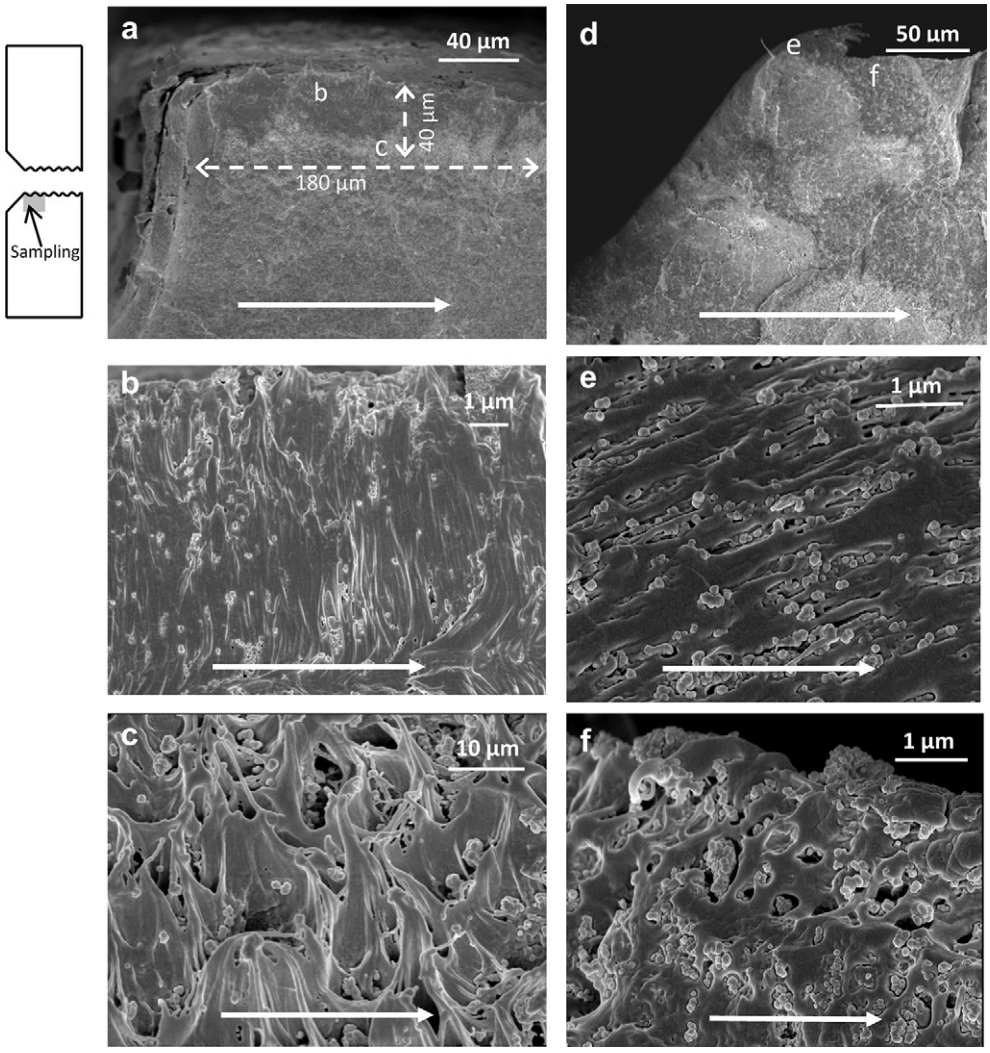

Fig. 7. SEM micrographs of the cross-sections underneath the fracture surfaces of impact-fractured E-5-20 and MA-5-20 impact bars. (a), (b) and (c) are SEM micrographs taken from E-5-20. (d), (e) and (f) are SEM micrographs taken from MA-5-20.

4. Conclusion

Numerous studies on the toughening mechanisms of rigid-particle-filled PP have identified that debonding was a key step to release the strain constraint and thus to trigger massive plastic deformation [5–8]. The major contribution of this current study is to point out that, given the occurrence of debonding, the ultimate impact toughness actually depends on the matrix properties to a great extent. High ligament strength is essential for high impact strength because strong ligaments can withstand higher fracture stresses and therefore allow for considerable plastic deformation, consuming a large amount of fracture energy. When comparing H-5-20 and E-5-20, even though debonding takes place in both nanocomposites, their impact strengths vary dramatically. The ligaments of H-5-20 underwent slight plastic deformation before they failed. Hence, the improvement in the impact strength was limited. In contract, strong ligaments of E-5-20 were capable to withstand high stresses, resulting in the enhancement of both the extent and scale of plastic deformation. The high ligament strength of E-5-20 was created by using a high-molecular-weight E-PP, due to its high density of tie molecules. Over the years, researchers have realized that high-molecular-weight polymers including thermosets [47] and thermoplastics [8,21–23,48] have better toughenability, which means that the composites with high-molecular-weight matrices have a better ability to be toughened while other parameters remain the same. However, the concept of 'better toughenability' has not been explicitly interpreted. As revealed by this study, the function of high-molecular-weight matrix is to provide high fracture stress, which stabilizes the plastic deformation in the crack-initiation stage. In addition, the effect of the molecular weight on the dispersion of nanoparticles was investigated. A high-molecular-weight polymer matrix does not necessarily ensure good dispersion of nanoparticles and a monolayer coating is an effective means to improve the dispersion of nanoparticles. The synergic effect of the high-molecular-weight PP and the monolayer-coated nanoparticles on the impact strength of PP/$CaCO_3$ nanocomposites has been demonstrated.

Acknowledgements

This study was financially supported by the Hong Kong Government Research Grants Council under grants 610906, 610907 and 621306. The assistance given by the Materials Characterization and Preparation Facility and the Advanced Engineering Materials Facility is highly appreciated. Special thanks are given to Japan Polypropylene for the supply of E-PP.

References

[1] LeBaron PC, Wang Z, Pinnavaia TJ. Appl Clay Sci 1999;15:11–29.
[2] Rong MZ, Zhang MQ, Zheng YX, Zeng HM, Walter R, Friedrich K. Polymer 2001;42:167–83.
[3] Xavier SF, Schultz JM, Friedrich K. J Mater Sci 1990;25:2411–20.
[4] Chan CM, Wu JS, Li JX, Cheung YK. Polymer 2002;43:2981–92.
[5] Kim GM, Michler GH, Gahleitner M, Fiebig J. J Appl Polym Sci 1996;60:1391–403.
[6] Kim GM, Michler GH. Polymer 1998;39:5689–97.
[7] Kim GM, Michler GH. Polymer 1998;39:5699–703.
[8] Zuiderduin WCJ, Westzaan C, Huetink J, Gaymans RJ. Polymer 2002;44:261–75.
[9] Thio YS, Argon AS, Cohen RE, Weinberg M. Polymer 2002;43:3661–74.
[10] Zhang QX, Yu ZZ, Xie XL, Mai YW. Polymer 2004;45:5985–94.
[11] Jancar J, Dibenedetto AT, Dianselmo A. Polym Eng Sci 1993;33:559–63.
[12] Price GJ, Ansari DM. Polym Int 2004;53:430–8.
[13] Ahsan T, Taylor DA. J Adhes 1998;67:69–79.
[14] Thio YS, Argon AS, Cohen RE. Polymer 2004;45:3139–47.
[15] Gensler R, Plummer CJG, Grein C, Kausch H-H. Polymer 2000;41:3809–19.
[16] Leong YW, Abu Bakar MB, Mohd.Ishak ZA, Ariffin A, Pukanszky B. J Appl Polym Sci 2004;91:3315–26.
[17] Zhang L, Li CZ, Huang R. J Polym Sci Part B Polym Phys 2004;42:1656–62.
[18] Lin Y, Chen HB, Chan CM, Wu JS. Macromolecules 2008;41:9204–13.
[19] Ishikawa M, Ushui K, Kondo Y, Hatada K, Gima S. Polymer 1996;37:5375–9.
[20] Wulin Qiu WL, Endo T, Hirotsu T. Eur Polym J 2006;42:1059–68.
[21] Moon CK. J Appl Polym Sci 1998;67:1191–7.
[22] González-Montiel A, Keskkula H, Paul DR. Polymer 1995;36:4587–603.
[23] Fornes TD, Yoon PJ, Keskkula H, Paul DR. Polymer 2001;42:9929–40.
[24] Oshinski AJ, Keskkula H, Paul DR. Polymer 1996;37:4891–907.
[25] Oshinski AJ, Keskkula H, Paul DR. Polymer 1996;37:4909–18.
[26] Oshinski AJ, Keskkula H, Paul DR. Polymer 1996;37:4919–28.
[27] Van Der Wal A, Mulder JJ, Oderkerk J, Gaymans RJ. Polymer 1998;39:6781–7.
[28] Clark EJ, Hoffman JD. Macromolecules 1984;17:878–85.
[29] Gahleitner M, Wolfschwenger J, Bachner C, Bernreitner K, Neißl W. J Appl Polym Sci 1996;61:649–57.
[30] Gahleitner M, Bernreitner K, Neißl W, Paulik C, Ratajski E. Polym Test 1995;14:173–87.
[31] Kinloch AJ, Young RJ. Fracture behavior of polymers. 1st ed. London and New York: Elsevier; 1983. p. 330.
[32] Stern C, Frick A, Weickert G. J Appl Polym Sci 2007;103:519–33.
[33] Keller A, Machin MJ. J Macromol Sci Phys 1967;1:41–91.
[34] Stern C, Frick AR, Weickert G, Michler GH, Henning S. Macromol Mater Eng 2005;290:621–35.
[35] Schrauwen BAG, Janssen RPM, Govaert LE, Meijer HEH. Macromolecules 2004;37:6069–78.
[36] Karger-Kocsis J. In: Karger-Kocsis J, editor. Polypropylene structure, blends and composites, vol. 3. London: Chapman & Hall; 1995. p. 146.
[37] Nitta KH, Takayanagi M. J Polym Sci Part B Polym Phys 1999;37:357–68.
[38] Peterlin A. J Mater Sci 1971;6:490–508.
[39] Móczó J, Fekete E, Pukánszky B. Progr Colloid Polym Sci 2004;125:134–41.
[40] Van Der Wal A, Mulder JJ, Thijs HA, Gaymans RJ. Polymer 1998;39:5467–75.
[41] Sugimoto M, Ishikawa M, Hatada K. Polymer 1995;36:3675–82.
[42] Avella M, Dell'Erba R, Martuscelli E, Ragosta G. Polymer 1993;34:2951–60.
[43] Irwin GR. Appl Mater Res 1964;3:65–81.
[44] Dugdale DS. J Mech Phys Solids 1960;8:100–8.
[45] Greco R, Ragosta G. J Mater Sci 1988;23:4171–80.
[46] Fukuhara N. Polym Test 1999;18:135–49.
[47] Lee J, Yee AF. Polymer 2000;41:8375–85.
[48] Lu M, Keskkula H, Paul DR. J Appl Polym Sci 1996;59:1467–77.